Identification and Reactivity of Cyclometalated Iron(II) Intermediates in Triazole-Directed Iron-Catalyzed C-H Activation

Theresa E. Boddie,[†] Stephanie H. Carpenter,[†] Tessa M. Baker,[†] Joshua C. DeMuth,[†] Gianpiero Cera,[‡] William W. Brennessel, [†] Lutz Ackermann,[‡] Michael L. Neidig*,[†]

Supporting Information Placeholder

ABSTRACT: While iron-catalyzed C-H activation offers an attractive reaction methodology for organic transformations, the lack of molecular-level insight into the in situ formed and reactive iron species impedes continued reaction development. Herein, freeze-trapped ⁵⁷Fe Mössbauer spectroscopy and single-crystal X-ray crystallography combined with reactivity studies are employed to define the key cyclometalated iron species active in triazole-assisted iron-catalyzed C-H activation. These studies provide the first direct experimental definition of an activated intermediate, which has been identified as the lowspin iron(II) complex $[(sub-A)(dppbz)(THF)Fe]_2(\mu-MgX_2)$, where sub-A is a deprotonated benzamide substrate. Reaction of this activated intermediate with additional diarylzinc leads to the formation of a cyclometalated iron(II)-aryl species, which upon reaction with oxidant, generates C-H arylated product at a catalytically relevant rate. Furthermore, pseudo single turnover reactions between catalytically relevant iron intermediates and excess nucleophile identify transmetalation as rate-determining. whereas C-H activation is shown to be facile, even at room temperature.

INTRODUCTION

The development of iron catalysts which directly activate and functionalize C-H bonds for the synthesis of high value molecules has been an area of intense research for over a decade, with iron attracting significant interest due to its low cost, limited toxicity, and rich oxidation chemistry. A key example in this area is work by Nakamura and co-workers which pioneered a substrate-directed approach to form new C-C bonds by coupling C-H bonds with organozinc reagents using an iron catalyst, ligand and 1,2-dichloroisobutane (DCIB) to afford high product yields (up to 99 %) under mild conditions (Scheme 1a). Following this seminal report, iron-catalyzed C-H functionalization methodologies have been expanded with key contributions from several groups, including Nakamura, Ackermann and Cook to achieve numerous chemical transformations, including allylation, alkylation, arylation, arylation, irallene and alkyne annulation, alkylation, arylation, arylation of varying $C(sp^2)$ -H¹⁹⁻²⁰ and $C(sp^3)$ -H bond types. 12, 21-22

Despite considerable advances in directed iron-catalyzed C-H transformations, detailed mechanistic understanding of these systems remains under developed and poorly understood in stark contrast to our understanding of directed C-H activation systems which utilize precious metals.²³ While Nakamura and co-workers have postulated the formation of a cyclometalated iron intermediate that is stabilized by substrate directing groups, ^{18, 21} no spectroscopic or structural evidence directly identifying this species has been reported. Instead, mechanistic knowledge is limited largely to theoretical studies as well as experimental observations such as C-C bond formation, unlike C-H activation, requires the presence of oxidant, and thus the oxidation of the iron center, for subsequent product formation.^{18,24} For the former, Shaik, Chen and co-workers have demonstrated

Scheme 1. Selected Examples of Iron-Catalyzed C-H Activation Reactions

[†]Department of Chemistry, University of Rochester, Rochester, New York 14627, United States

[‡]Institut für Organische und Biomolekulare Chemie, Georg-August-Universität Göttingen, Tammannstraße 2, 37077, Gottingen, Germany

computationally that the most efficient catalytic cycles for these systems involve the evolution of iron oxidation state through either Fe(II)/Fe(II)/Fe(I) or Fe(II)/Fe(0) cycles. ²⁴ While these theoretical insights identify possible oxidation states of iron intermediates that might be accessible, the ability of iron to adopt multiple oxidation and spin states as well as coordination geometries necessitate direct experimental studies to define the iron intermediates involved in catalysis.

Previous efforts to obtain molecular-level insight into the mechanism of catalysis in these systems were significantly limited due to the lack of direct spectroscopic and structural insight into the nature of the in situ formed iron species. The current study addresses these critical challenges by utilizing an experimental approach combining freeze-trapped inorganic spectroscopic methods including ⁵⁷Fe Mössbauer spectroscopy and single-crystal X-ray diffraction (SCXRD) with concurrent reactivity and kinetic studies. ²⁵⁻²⁶ Previously applied to iron-catalyzed cross-coupling, ²⁷⁻²⁹ herein this approach is used to define in situ iron speciation, reactivity and mechanism operative in iron-catalyzed arylation of C(sp²)-H bonds by triazole assistance (Scheme 1d)¹². The current study is the first to identify and characterize key cyclometalated iron(II) intermediates in this system, including their coordination environments, rates of formation and reaction pathways leading to C-C bond formation during catalysis.

RESULTS AND ANALYSIS

Identification of a Substrate-Bound High-Spin Iron(II) **Complex.** Initial studies utilized freeze-trapped 80 K ⁵⁷Fe Mössbauer spectroscopy to evaluate iron speciation in stoichiof ⁵⁷Fe(acac)₃, reactions 1,2-bis(diphenylphosphino)benzene (dppbz) and N-{2-[1-benzyl-1H-1,2,3triazol-4-yl|propan-2-yl}-2-methylbenzamide (H-sub-A) (Fig 1) with various equivalents of in situ generated Ar_2Zn (Ar = 4-MeOC₆H₄) [from the Grignard reagent ArMgBr and $ZnBr_2 \cdot TMEDA$ (TMEDA = N, N, N', N'-tetramethylethylenediamine)] with the aim to form cyclometalated iron intermediates previously proposed,³⁰ but never identified for related systems.^{18, 21} Note that all stoichiometric reactions are performed with enriched ⁵⁷Fe at the concentration observed in catalysis (~8.3 mM) to enable analysis by freeze-trapped solution ⁵⁷Fe Mössbauer spectroscopy. A solution of 1 equiv each of H-sub-A and Ar₂Zn in THF was stirred for 10 min at RT, followed by the subsequent addition of a mixture containing ⁵⁷Fe(acac)₃ and dppbz in THF at RT. Freeze-trapped ⁵⁷Fe Mössbauer spectroscopy after 10 minutes of reaction at 55 °C (the temperature employed in catalysis) of the resulting yellow solution indicated the formation of one predominate iron species with Mössbauer parameters of $\delta = 0.94$ mm/s and $\Delta E_0 = 3.14$ mm/s (1, Fig 1A), consistent with the formation of a high-spin iron(II) complex.³¹ Analogous ⁵⁷Fe Mössbauer studies indicate that 1 is stable at 55 °C for over 45 minutes in THF. The addition of dppbz to the reaction mixture has no effect, suggesting that dppbz does not coordinate to 1 (Fig S1). Consequently, iron species 1 can also be generated under conditions in which H-sub-A is deprotonated with n-BuLi and subsequently added to FeCl₂ in THF, also at 55 °C (Fig S2).

Despite extensive efforts, crystalline material of **1** suitable for SCXRD could not be obtained. However, the generation of **1** as the only observable iron species in solution (via ⁵⁷Fe Mössbauer) enabled spectroscopic studies to further define its oxidation state, coordination number, geometry and spin state using

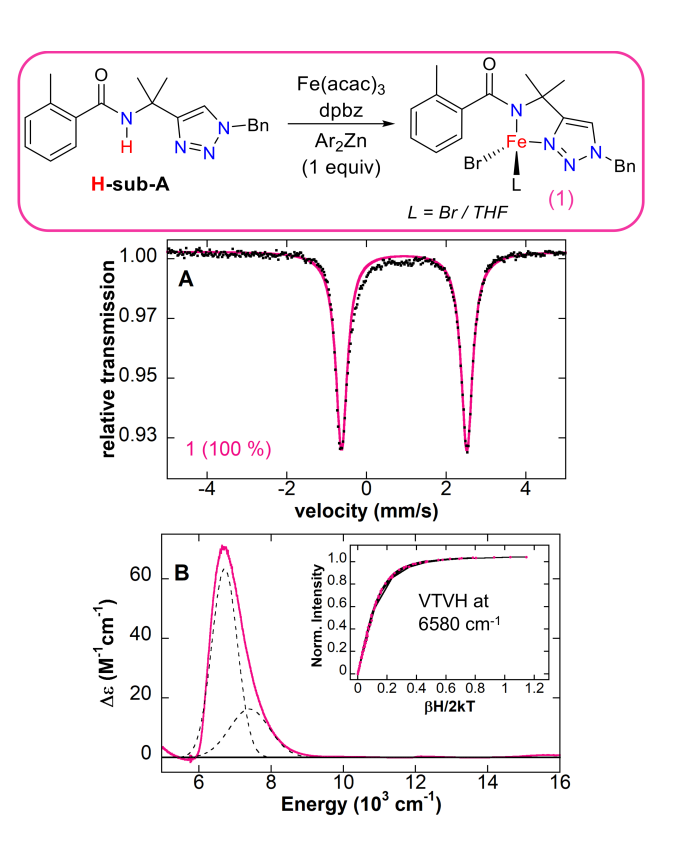


Figure 1. ⁵⁷Fe Mössbauer and MCD spectroscopy of the in situ formed iron species from the reaction of Fe(acac)₃, dppbz and H-sub-A with 1 equiv of Ar₂Zn. (A) The 80 K ⁵⁷Fe Mössbauer and (B) 5 K, 7 T NIR MCD spectrum with inset of VTVH-MCD of **1** (8.3 mM) in (A) THF and (B) 1:1 THF/2-MeTHF. Saturation magnetization data (dots) and best fit (lines) collected at 6580 cm⁻¹. Peak fits are shown for the MCD spectra (dashed lines). Inset scheme describes stoichiometry employed, as well as the proposed structure of **1**.

magnetic circular dichroism (MCD) spectroscopy. The 5 K, 7 T near-infrared (NIR) MCD spectrum of 1 in 1:1 THF/2-MeTHF is dominated by two low energy ligand-field transitions at \sim 6710 cm⁻¹ and \sim 7400 cm⁻¹ (10 $Dq(T_d) = 7055$ cm⁻¹), indicative of a four-coordinate distorted tetrahedral complex (Fig 1B).³ Saturation magnetization data for 1 collected at 6580 cm⁻¹ are well-described by a S = 2 negative zero-field split (-ZFS) non-Kramers doublet model with ground-state spin-Hamiltonian parameters of $\delta = 1.5 \pm 0.2 \text{ cm}^{-1}$ and $g_1 = 9.0 \pm 0.2 \text{ with } D = -11 \pm 0.2 \text{ m}^{-1}$ 2 cm^{-1} and $|E/D| = 0.22 \pm 0.06$ (Fig 1B, inset). These studies combined with the reaction stoichiometry employed to generate 1 (1:1 iron to H-sub-A without dppbz) and the lack of ²H-NMR resonance in the aryl region when quenched with D₂O (see SI), enabled its assignment as a distorted tetrahedral, high-spin iron(II) species of either the general formula [Fe^{II}(sub-A)Br₂] or [Fe^{II}(sub-A)(Br)(THF)], where sub-A denotes the benzamide substrate deprotonated at the amide position. The second formula is included since the ligation of a solvent molecule could not be excluded.

Synthesis, Spectroscopic Characterization and Reactivity of Activated Low-Spin Iron(II) Intermediates. Whereas stoichiometric reactions with 1 equiv of Ar₂Zn led to formation of 1, analogous reactions in the presence of 2 equiv of Ar₂Zn resulted in further reaction of 1 with a concurrent color change from yellow to green. Freeze-trapped 80 K ⁵⁷Fe Mössbauer

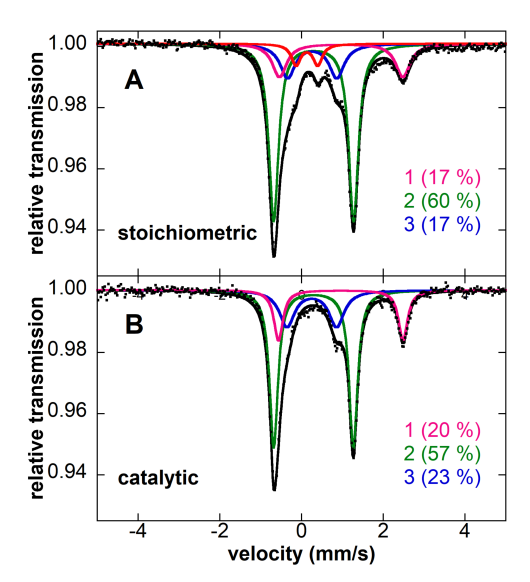


Figure 2. Freeze-trapped ⁵⁷Fe Mössbauer spectra of frozen solutions of Fe(acac)₃, H-sub-A and dppbz under (A) stoichiometric conditions with 3 equiv of Ar₂Zn observed at 80 K and (B) catalytic conditions observed at 5 K. Total fit (black line) and individual fit components are shown.

spectroscopy after extended reaction time (1 h) at 55 °C indicated the formation of 1 (47 % of all iron), as well as two additional iron species characterized by Mössbauer parameters of δ = 0.30 mm/s and ΔE_Q = 1.92 mm/s (iron species 2, 43 % of all iron, green component) and δ = 0.24 mm/s and ΔE_Q = 1.19 mm/s (iron species 3, 10 % of all iron, blue component). Interestingly, the isomer shifts of 2 and 3 were suggestive of six-coordinate low-spin iron(II) species in the presence of strong ligand fields (vide infra, Fig S3 and Table 1). In contrast to 1, formation of 2 and 3 requires dppbz to be present. To target increased amounts of these low-spin iron species, a similar stoichiometric reaction was performed utilizing 3 equiv of $\Delta r_2 Zn$ with the hy-

pothesis that the added nucleophile would consume remaining 1 to generate additional 2 and 3. Consistent with this hypothesis, freeze-trapped 80 K 57 Fe Mössbauer spectroscopy after 30 minutes of reaction with 3 equiv of Ar $_2$ Zn at 55 °C indicated a decreased amount of 1 (17% of all iron), as well as increased amounts of both low-spin iron(II) species 2 and 3, 60 % (green component) and 17 % (blue component), respectively (Fig 2A). A fourth minor iron species 4 with parameters $\delta=0.15$ mm/s and $\Delta E_Q=0.54$ mm/s (6 %, red component) is generated in the presence of excess Ar $_2$ Zn (> 3 equiv, vide infra). Notably, spin-quantitated 5 K electron paramagnetic resonance (EPR) spectroscopy showed a S=1/2 iron species also formed, but only represented \leq 1% of all iron in solution and therefore below the detection limits of 57 Fe Mössbauer spectroscopy (~ 3 %).

To determine whether the previously defined iron species are also present during catalysis, the catalytic reaction was performed following the reported protocol, ¹² and the iron speciation was evaluated using freeze-trapped ⁵⁷Fe Mössbauer spectroscopy. Due to excess salts present in solution in catalysis (30 equiv of Zn with respect to 1 equiv of Fe), ⁵⁷Fe Mössbauer samples were analyzed at 5 K for improved spectral resolution (see Fig S4 for spectrum at 80 K). At 21 h into the 36 h catalytic reaction, **2** was present as the major component (57% of iron) in solution with contributions from **1** and **3** as well (20% and 23%, respectively, Fig 2B). Spin-quantitated 5 K EPR spectroscopy indicated that < 0.5 % of all iron in solution during catalysis was S = 1/2. Thus, it was clear that iron species **2** and **3** are potential key intermediates in catalysis, and further characterization was pursued.

As **2** was the major species observed in situ in both stoichiometric and catalytic reactions, extensive efforts were focused towards its isolation and structural characterization. However, crystallization of **2** was impeded by the formation of crystalline zinc salt. To this end, a separate stoichiometric protocol using ArMgBr to form **2** was developed to avoid zinc salt production. Freeze-trapped 80 K ⁵⁷Fe Mössbauer spectroscopy of the addition of dppbz and ArMgBr (1 equiv each) to sub-A (deproto-

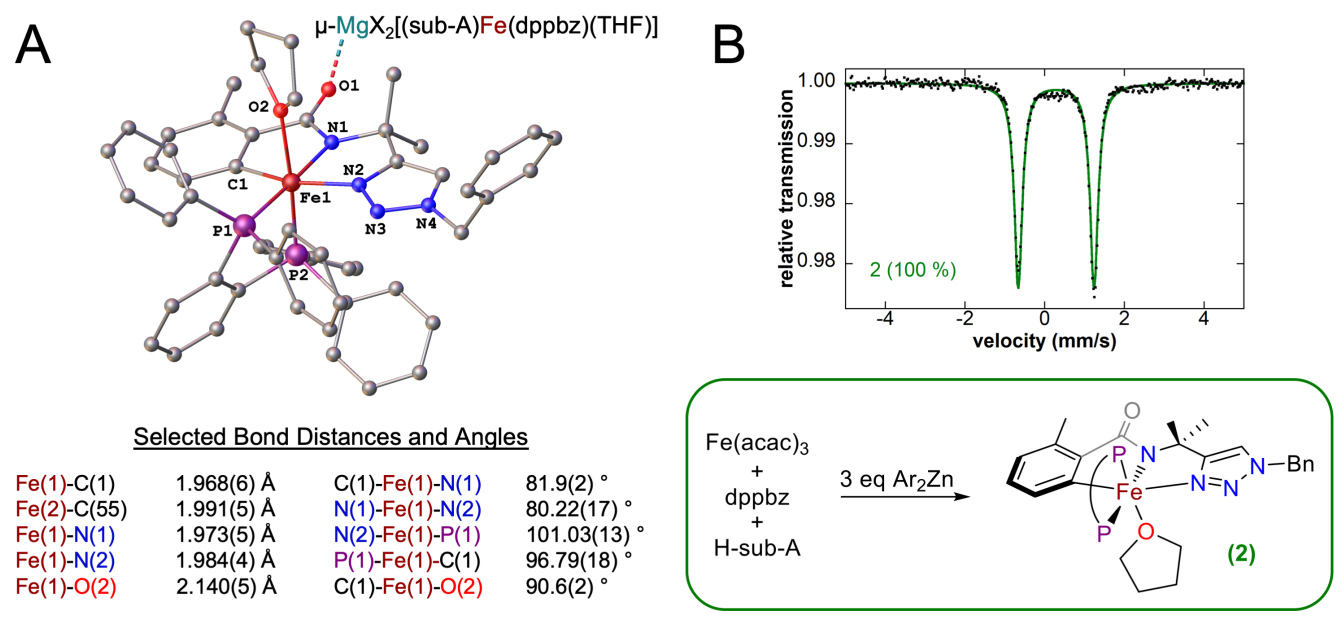


Figure 3. (A) Partial spheroid plot and (B) solid-state 5 K 57 Fe Mössbauer spectrum of 57 Fe-enriched crystalline [(sub-A)(dppbz)(THF)Fe]₂(μ -MgX₂) (2) with selected bond lengths and angles. For clarity purposes, the second monomer, which is connected via a MgX₂ bridge at O1, is included as text. Inset scheme describes the stoichiometry employed, as well as simplified connectivity of 2. See SI for full X-ray crystal structure report, which includes the anisotropic displacement ellipsoid plot.

Table 1. 80 K ⁵⁷Fe Mössbauer parameters of identified iron species relating to triazole-directed iron-catalyzed C-H activation.

Complex	Sample	$\delta (\text{mm s}^{-1})$	$\Delta E_Q (\text{mm s}^{-1})$
This work			
1	Frozen soln	0.94	3.14
2	Frozen soln	0.30	1.92
	Solid ^(5K)	0.30	1.90
3	Frozen soln	0.24	1.19
4	Frozen soln	0.15	0.54
4*	Frozen soln	0.17	0.56
	Solid	0.17	0.55
5	Frozen soln	0.43	1.70
Previously reported			
Fe(η ⁶ -biphenyl)(SciOPP)	Frozen soln	0.44	1.75

nated from n-BuLi) and FeCl₂ in THF at RT resulted in a distribution of iron species 1, 2 and 3, as previously observed in stoichiometric and catalytic reactions (Fig S5). Air- and moisturesensitive green crystalline needles suitable for SCXRD were obtained from recrystallization of this iron distribution in a mixture of anisole and THF at -30 °C, permitting the assignment of a cyclometalated iron(II) dimer [(sub-A)(dppbz)(THF)Fe]₂(µ- MgX_2) (2), where X = Cl or Br (due to halide exchange), in which a magnesium salt bridges two neutral monomers (Fig 3). Each iron center is coordinated to sub-A (tridentate ligation) and dppbz, as well as one THF molecule cis to the activated Fe-C bond in a distorted octahedral geometry. Note that the activated iron- $C(sp^2)$ bond lengths, 1.968(6) and 1.991(5) Å, are longer than the reported activated Co(III)- $C(sp^2)$ bonds with similar directing groups (Table S1). The 5 K ⁵⁷Fe Mössbauer spectrum of crystalline material exhibited parameters of δ = 0.30 mm/s and $\Delta E_O = 1.90$ mm/s (Fig 3B), confirming that this complex represents the major iron species 2 found to form in situ in stoichiometric and catalytic reactions. Note that the very small change in ΔE_0 in the solid state spectrum is consistent with a slight structural distortion between the solid and solution states, as previously observed for other iron-bisphosphine complexes.33

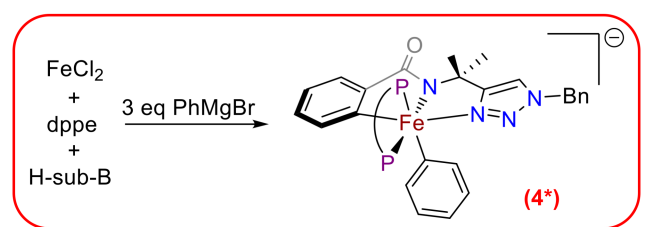
Since both 2 and 3 have similar isomer shifts and exist in a consistent ratio under stoichiometric and catalytic conditions, suggesting they potentially exist in equilibrium, it was proposed that 3 might correspond to the five-coordinate, non-THF ligated analog of 2. Further, both 2 and 3 are simultaneously consumed in reaction studies with excess nucleophile as expected for related species (vide infra). To test this hypothesis, 2 was generated in situ utilizing the crystallization protocol and dried in vacuo. The remaining green residue was re-dissolved in 2-MeTHF, resulting in 3 as the major species by Mössbauer spectroscopy (up from 19% to 80%, Fig S6). Thus, 2 can be assigned as the THF adduct of 3. Lastly, to further probe the spin states of 2 and 3, NMR spectra (¹H, ³¹P and ²H) were collected on the generated mixture and found to be consistent with the presence of two activated low-spin iron(II) species, as suggested by the previously defined Mössbauer parameters (see SI).

While 2 represents the first structurally characterized, cyclometalated iron species shown to form under both stoichiometric and catalytic conditions in directed iron-catalyzed C-H activation reactions, it is noteworthy that 2 and 3 lack coordination of an aryl ligand as likely required for C-C bond formation. It is therefore not surprising that in situ generated 2 and 3 show

no product formation by LC-MS analysis upon quenching. Interestingly, neither 2 or 3 react with DCIB as determined by freeze-trapped ⁵⁷Fe Mössbauer spectroscopy (Fig S7), consistent with the observation of these species during catalysis in the presence of excess DCIB.

Finally, pseudo single turnover studies of the reaction of 1 with excess nucleophile to generate cyclometalated intermediates 2 and 3 were conducted to determine their rate of formation using time-resolved, freeze-quenched ⁵⁷Fe Mössbauer spectroscopy as previously employed in iron cross-coupling chemistry. ³³ At catalytic temperature (55 °C), the formation of 2 and 3 results from reaction of 1 and excess Ar_2Zn (14 equiv) at an observed rate constant of $0.26 \pm 0.03 \text{ min}^{-1}$ via a pseudo-first order kinetic fit (Fig S8-9). Interestingly, cyclometalated intermediate 2 can be generated at room temperature from reaction of 1 with dppbz and 14 equiv of Ar_2Zn (within 8 min), suggesting that C-H activation is facile and does not require heating (Fig S10).

Identification of an Arylated, Cyclometalated Iron(II) Complex for C-C Product Formation. It was hypothesized that an arylated analog of 2, where the THF ligand is replaced



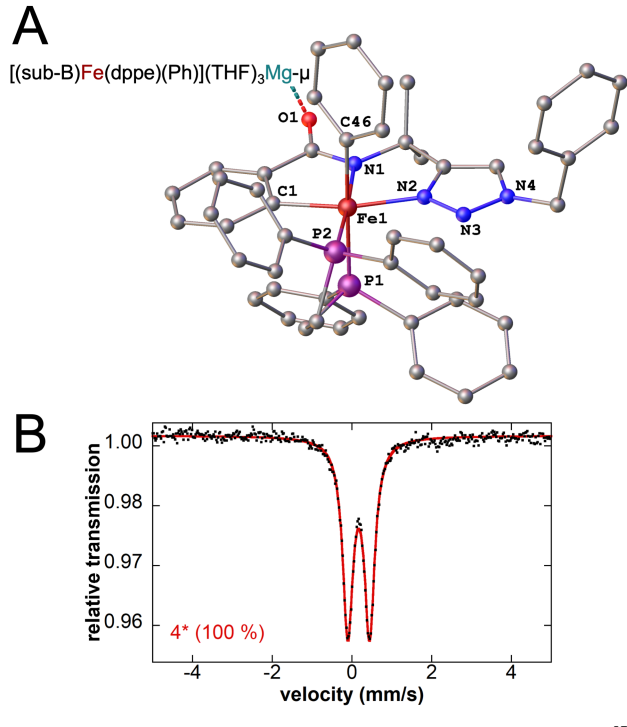


Figure 4. (A) Partial spheroid plot and (B) solid-state 80 K ⁵⁷Fe Mössbauer spectrum of ⁵⁷Fe-enriched crystalline [(sub-B)(dppe)(Ph)Fe]₂(μ-Mg(THF)₃) (**4***). The second monomer, which is connected via a Mg(THF)₃ bridge at O1, is added in text. Inset scheme describes the stoichiometry employed, as well as simplified connectivity of **4***. See SI for full X-ray crystal structure report, which includes the anisotropic displacement ellipsoid plot.

by an aryl ligand (4-MeOC₆H₄), might be accessible upon further reaction with Ar₂Zn. Furthermore, such a species might be effective for C-C bond formation due to the coordination of the aryl group near the activated Fe-C(sp²) bond. Towards such a species, stoichiometric addition of 2 equiv of Ar₂Zn in THF to a solution of 2 and 3 was performed, resulting in a slow color change from green to red over 80 minutes at 55 °C. Freezetrapped 80 K ⁵/Fe Mössbauer spectroscopy indicated the formation of two additional iron species with Mössbauer parameters of $\delta = 0.15$ mm/s and $\Delta E_0 = 0.54$ mm/s (iron species 4, 71 % of all iron, red component) and $\delta = 0.43$ mm/s and $\Delta E_0 = 1.70$ mm/s (iron species 5, 7 % of all iron, purple component), as well as unreacted 2 and 3 (26 % and 6 % of all iron, respectively) (Fig S11, for 44 min and 80 min timepoints). Spin-quantitated 5 K EPR spectroscopy indicated that < 0.5 % of all iron in solution during in situ generation of 4 was S = 1/2. Notably, iron species 5 has Mössbauer parameters similar to those of iron(0) complexes, specifically Fe(η^6 -biphenyl)(dppbz) (Fig S12) and Fe(η^6 -biphenyl)(SciOPP),³³ suggesting the assignment Fe(n⁶-biaryl)(dppbz) (see Table 1). Analogous ⁵⁷Fe Mössbauer studies indicate that 4 is stable at 55 °C for up to 2 h and in the presence of additional Ar_2Zn (10 equiv, see Fig S13).

Efforts to crystallize 4 under these conditions were unsuccessful. Interestingly, an iron species with nearly identical Mössbauer parameters to 4 was found to form in an analogous triazole-assisted iron-catalyzed C-H functionalization system 1 equiv each of FeCl₂, 1,2-bis(diphenylphosphino)ethane (dppe) and N-(2-[1-benzyl-1H-1,2,3-triazol-4-yl]propan-2-yl)benzamide (H-sub-B) reacted with 3 equiv PhMgBr (see Scheme 1e). Freeze-trapped solution 80 K ⁵⁷Fe Mössbauer spectroscopy of these stoichiometric conditions indicate the formation of one predominate iron species (4*) characterized by $\delta = 0.17$ mm/s and $\Delta E_0 = 0.56$ mm/s (97 % of all iron, Fig S14). Fortunately, these conditions allowed for the formation of air- and moisture-sensitive orange-red crystalline needles obtained from a mixture of hexanes and THF at -30 °C. SCXRD identified the structure of 4* as the cyclometalated low-spin iron(II)-phenyl dimer, $[(sub-B)(dppe)(Ph)Fe]_2(\mu-dpe)$ Mg(THF)₃) (Fig 4A). Notably, the iron monomers are chargebalanced with a Mg(THF)₃²⁺ bridge, allowing the dimer to have an overall neutral charge. Furthermore, each iron center is coordinated to sub-B and dppe and has replaced the THF molecule with a phenyl molecule cis to the activated Fe-C bond in a distorted octahedral geometry. The activated iron- $C(sp^2)$ bond lengths, 1.976(3) and 1.981(3) Å, are like those seen in 2 though slightly shorter than the iron-Ph bond lengths, 2.036(3) and 2.039(3) Å. The 80 K ⁵⁷Fe Mössbauer spectrum of crystalline **4*** is defined by $\delta = 0.17$ mm/s and $\Delta E_Q = 0.55$ mm/s (Fig 4B, see Fig S15 for solution). NMR (¹H and ³¹P) spectra were collected on crystalline 4* in THF-d⁸ and are consistent with lowspin iron(II) (see SI).

From the unambiguous structure of **4***, as well as 57 Fe Mössbauer analysis, **4** is assigned as the cyclometalated iron(II)-aryl analog of **2** (i.e. aryl replaces THF). To evaluate the rate of transmetalation of the aryl group, pseudo single turnover studies of in situ generated **4** from cyclometalated species **2** and **3** were conducted with 14 equiv of Ar₂Zn at 55 °C and tracked by freeze-trapped ⁵⁷Fe Mössbauer spectroscopy as a function of time (Fig S16). From a pseudo-first order kinetic fit, the observed rate constant of 0.06 ± 0.03 min⁻¹ was estimated (Fig S17), signifying that transmetalation occurred slower than C-H activation though still sufficiently fast for catalytic relevance (average turnover time of ~0.01 min⁻¹ during catalysis).

The presence of aryl ligand and cyclometalated substrate in 4 suggested that this species might be competent for C-C bond formation. Therefore, reactivity studies using stoichiometric reactions of 4 with excess Ar₂Zn and DCIB were conducted. Freeze-trapped ⁵⁷Fe Mössbauer spectroscopy was used to determine that 72 % of all iron initially present in stoichiometric conditions involving 5 equiv of Ar₂Zn at extended reaction time (90 min) at 55 °C was 4, in addition to small contributions from 5 (14 %), 2 (8 %) and 3 (5 %) (Fig S18). Aliquots of the in situ distribution with and without 1 equiv of DCIB were chemically quenched and analyzed by LC-MS analysis, which both showed product formation (72 %) equal to the amount of 4 in solution. Given that there is no change of iron speciation by ⁵⁷Fe Mössbauer spectroscopy upon heating 4 for extended time periods (i.e. no reaction), the product formation in the absence of DCIB is attributed to the oxidation event of the quench rather than the reductive elimination of iron. Thus, quantitated spectroscopic methods which directly assess iron speciation are more reliable in this case to evaluate in situ formed iron speciation than quantitation of organic products, which can artificially form due to quenching procedures.^{29, 34} Lastly, following the addition of DCIB (1 equiv) to in situ 4 (72 % of all iron) at 55 °C for an extended reaction time (50 min), freeze-trapped ⁵⁷Fe Mössbauer analysis showed consumption of 4 and 5 (45 % and 14 %, respectively), as well as the formation of a plethora of Fe(II) species (Fig S18). Notably, the in situ quantities of activated iron species 2 and 3 increase by a total sum of 14 %, suggesting that iron(0) complex 5 was oxidized by DCIB and re-entered the catalytic cycle. To determine the observed rate of reaction with oxidant, Fe(acac)₃ and dppbz in THF were added to a stirring solution of H-sub-A with 5 equiv of Ar₂Zn and reacted at 55 °C for 80 minutes prior to the addition of 20 equiv DCIB (equivalents of oxidant to iron under catalytic conditions). Consumption of the arylated iron intermediate 4 by reaction with DCIB was estimated by freeze-trapped, time-resolved ⁵⁷Fe Mössbauer studies to occur at an observed rate constant of $0.18 \pm 0.04 \text{ min}^{-1}$ under pseudo-first order conditions (Fig S19-20). Conversely, separate studies were conducted with complex 5 and DCIB. FeCl₂ and dppbz were reacted with 5 equiv of ArMgBr to form one predominate iron species with matching Mössbauer parameters of complex 5 ($\delta = 0.43$ mm/s, $\Delta E_Q = 1.70$ mm/s, Fig S21). Reaction of in situ generated 5 (> 99 % of all iron) with 20 equiv DCIB in THF at 55 °C results in rapid consumption of 5 ($k_{obs} \ge$ 5 min⁻¹) to generate iron(II)-bisphosphine complexes, a reaction rate far in excess of the rate of cyclometalated iron-aryl species 4 with oxidant.

DISCUSSION

In the present study, the use of freeze-trapped ⁵⁷Fe Mössbauer, MCD and EPR spectroscopies combined with synthetic and reaction studies defines the in situ formed iron species in triazole-assisted iron-catalyzed C-H activation. These studies provide the first direct spectroscopic and structural insight into the nature of activated cyclometalated iron species central to this catalysis, including critical insight into their molecular structures, oxidation and spin states and their chemical transformations with Ar₂Zn and oxidant. The major iron species identified to form in situ and their observed transformations are summarized in Scheme 2.

Detailed spectroscopic studies suggest that the initial reaction with Ar₂Zn reduces Fe(III) to Fe(II) and generates a substrate-bound, but non-activated intermediate of general formula

Scheme 2. Summary of observed iron intermediates and their reactive transformations in triazole-assisted iron-catalyzed C-H activation

Fe(acac)₃
H-sub-A

$$Ar_2Zn$$

$$dppbz$$

$$sub-A$$

$$Fe'' N$$

$$not observable$$

$$Fe''' N = M$$

$$not observable$$

$$Fe''' N = M$$

$$Ar_2Zn$$

$$dppbz$$

$$k_{obs} = 0.26 \pm 0.03 \text{ min}^{-1}$$

$$Ar_2Zn$$

$$k_{obs} = 0.26 \pm 0.03 \text{ min}^{-1}$$

$$Ar_2Zn$$

$$N = M$$

$$N$$

[Fe(sub-A)X₂] or [Fe(sub-A)(X)(THF)]. In the presence of dppbz and excess Ar_2Zn , C-H activation to the octahedral lowspin iron(II) dimer [(sub-A)(dppbz)(THF)Fe]₂(μ-MgX₂), as well as its non-THF adduct analog, is facile, even at room temperature. The quick generation of these cyclometalated intermediates precludes any definitive spectroscopic evidence of possible intermediates between 1 and 2/3 in stoichiometric reactions. However, it is hypothesized that C-H activation may proceed via arylation of 1 followed by subsequent activation coupled to methoxybenzene formation, as previously proposed in computational studies by Shaik and Chen. 24

Further reaction of **2** and **3** with additional Ar₂Zn leads to transmetalation to a cyclometalated iron(II)-aryl complex. Generated at a catalytically relevant rate, though slow in contrast to activation, **4** reacts with DCIB to yield quantitative product formation, indicating that **4** is the reactive species for C-C product formation. It is interesting to note that at room temperature, the generation of this arylated intermediate is extremely slow (only 20 % of all iron after 1 h of reaction time) (Fig S9). Therefore, the high temperature in catalysis is likely needed for the formation of **4**, and hence for efficient C-C bond formation. The observation that transmetalation has a high activation barrier and is rate-determining is consistent with both previous calculations²⁴ and the in situ speciation during catalysis (activated iron intermediates **2** and **3** are present in high quantities while the iron-aryl species **4** is not visible, see Fig. 2).

Finally, stoichiometric reactions of in situ generated 4 and 5 with DCIB provide additional insight into the roles of the oxid-

ant in catalysis. First, DCIB serves to oxidize off-cycle, reduced iron species, such as 5, and transient on-cycle Fe(I) species (vide infra), which then re-enter the catalytic cycle. Furthermore, DCIB promotes a reductive elimination pathway, as previously observed for other systems. ¹⁷ Given that **4** does not react in the absence of oxidant, a catalytic cycle involving the reductive elimination of Fe(II) to generate Fe(0) is unlikely. Rather, stoichiometric reactions suggest that the catalytic cycle proceeds through Fe(II)/Fe(III)/Fe(I), as previously proposed by detailed DFT mechanistic studies.²⁴ Here, 4 reacts with DCIB to generate a transient Fe(III) complex, which reductively eliminates to form Fe(I) and product. Given that neither a Fe(III) or Fe(I) complex is observed, even during catalysis, the oxidation step from cyclometalated iron(II)-aryl to iron(III) must be slow in comparison to reductive elimination and subsequent oxidation of Fe(I). While the mechanism of this initial oxidation to Fe(III) is not clear, it could proceed via outer-sphere oxidation or displacement of a phosphine ligand.

Future studies will be directed towards the elucidation of the mechanism underlying the C-C bond forming step, with specific focus towards the identification of these exceptionally transient Fe(III) and Fe(I) species. Lastly, it is interesting to note that similar cyclometalated iron(II)-aryl intermediates are accessible under varying reaction conditions (i.e. Ar_2Zn vs. ArMgBr and dppbz vs. dppe), suggesting that directed iron-catalyzed C-H activation reactions may more broadly proceed through related intermediates.

CONCLUSION

A key cyclometalated intermediate in the iron-catalyzed arylation of $C(\mathsf{sp}^2)\text{-H}$ bonds by triazole assistance was isolated and identified as the diamagnetic iron(II) dimer [(sub-A)(dppbz)(THF)Fe]_2(\mu\text{-Mg}X_2). Reaction of this cyclometalated intermediate with Ar_2Zn leads to the formation of a cyclometalated low-spin iron(II)-aryl complex during the rate-determining catalytic transformation. The role of oxidant in these iron-catalyzed directed C-H activations is twofold, in that it reacts with the cyclometalated iron-aryl intermediate for C-H arylated product formation and re-oxidizes iron(I) and iron(0) complexes.

EXPERIMENTAL SECTION

General Considerations. Starting materials were synthesized according to previously described methods. ^{12, 35} All reagents were purchased from commercial sources and were used without further purification. ⁵⁷Fe(acac)₃ and ⁵⁷FeCl₂ were synthesized following a literature procedure using ⁵⁷Fe metal (95% enriched) purchased from Isoflex. All air and moisture sensitive manipulations were carried out in a MBraun inert-atmosphere N₂) glovebox equipped with a direct liquid nitrogen inlet line. All anhydrous solvents were freshly dried using activated alumina and 4Å molecular sieves and stored under inert-atmosphere.

⁵⁷Fe Mössbauer Spectroscopy. The solid samples 2 and 4* for ⁵⁷Fe Mössbauer spectroscopy were made from ⁵⁷Fe-enriched material and isolated from solvent. Dilute freeze-trapped solution samples for ⁵⁷Fe Mössbauer were prepared from ⁵⁷Fe(acac)₃ or ⁵⁷FeCl₂ to enable data collection. All samples were prepared in an inert-atmosphere glovebox equipped with a liquid nitrogen inlet line to freeze samples to 77 K within the glovebox. Each sample was loaded into a Delrin Mössbauer sample cup for analysis and loaded under liquid nitrogen. ⁵⁷Fe Mössbauer measurements were performed using a SeeCo. MS4 Mössbauer spectrometer integrated with a Janis SVT-400T He/N₂ cryostat for measurements at 5 and 80 K with a 0.07 T applied magnetic field. Isomer shifts were determined relative to α-Fe at 298 K. All Mössbauer spectra were fit using the program WMoss (SeeCo). Errors of the fit analyses were the following: $\delta \pm 0.02$ mm/s and $\Delta E_0 \pm 3\%$. For multicomponent fits, the quantitation errors were $\pm 3\%$ (e.g., $50 \pm 3\%$).

Magnetic Circular Dichroism (MCD) Spectroscopy. All samples for MCD spectroscopy were prepared in an inert-atmosphere glovebox equipped with a liquid nitrogen fill port to enable sample freezing to 77 K within the glovebox. MCD samples were prepared in 1:1 (v/v) THF / 2-MeTHF (to form low temperature optical glasses) in copper cells fitted with quartz disks and a 3 mm gasket. Low temperature near-infrared (NIR) experiments were conducted with a Jasco J-730 spectropolarimeter and a liquid nitrogen cooled InSb detector. A modified sample compartment incorporating focusing optics and an Oxford Instruments SM4000-7T superconducting magnet/cryostat was utilized. This setup permits measurements from 1.6 to 290 K with magnetic fields up to 7 T. A calibrated Cernox sensor directly inserted in the copper sample holder is used to measure the temperature at the sample to 0.001 K. All MCD spectra were baseline-corrected against zero-field scans. VTVH-MCD spectra were analyzed using previously reported fitting procedures. 32, 36

Electron Paramagnetic Resonance (EPR) Spectroscopy. Catalytic reaction solution samples for EPR spectroscopy were prepared directly from the reaction mixture as reported in literature under N₂ atmosphere. ¹² In situ stoichiometric reaction samples were prepared directly from the reactions as described. All samples for EPR spectroscopy were prepared in an inertatmosphere glovebox equipped with a liquid nitrogen inlet line to enable sample freezing to 77 K within the glovebox. EPR samples for spin integration were prepared in high precision 4 mm OD Suprasil quartz EPR tubes from Wilmad Labglass to allow for direct comparison of intensities between different samples. X-band EPR spectra were recorded on a Bruker EMXplus spectrometer equipped with a 4119HS cavity and an Oxford ESR-900 helium flow cryostat. The instrumental parameters employed for all samples were as follows: 1 mW (power), 41 ms (time constant), 8 G (modulation amplitude), 9.38 GHz (frequency) and 100 kHz (modulation frequency). Samples exhibiting S = 1/2 EPR spectra were spin integrated using an 8.3 mM CuSO₄ standard under non-saturating conditions. Identical instrumentation parameters were used for both iron and standard samples.

Liquid chromatography mass spectrometry (LC-MS). LC-MS measurements were performed using an Agilent Technologies 1260 Infinity II liquid chromatogram with a Restek Ultra C18 column and Advion Expression L mass spectrometer utilizing the electron spray ionization method. All LC-MS samples were made to a concentration of 1 mM. Details of method used were as follows: 5 μ L (injection volume), 1:1 water / acetonitrile with 0.1 % methanol (solvent mixture) and 28 minutes (total run time).

¹H, ²H and ³¹P Nuclear Magnetic Resonance (NMR) spectroscopy. Spectra were recorded on a Bruker 400 MHz at ambient temperature. Chemical shifts (δ) were recorded in parts per million (ppm) and, in the case of ¹H NMR, were referenced relative to residual solvent and solvent peaks (d^8 -THF 1.73 / 3.58).

ASSOCIATED CONTENT

The Supporting Information is available free of charge on the ACS Publications website. Experimental methods and supplementary data including Mössbauer, EPR, NMR and X-ray crystal details of 2 and 4* (PDF) X-ray crystallographic data for 2, 4* and Fe(η^6 -biphenyl)(dppbz)

AUTHOR INFORMATION

Corresponding Author

*neidig@chem.rochester.edu

Notes

The authors declare no competing financial interests.

ACKNOWLEDGMENT

This work was supported by grants from the National Science Foundation (CHE-1454370) to M. L. N., a NSF Graduate Research Fellowship to T. M. B. and Alexander Von Humboldt Foundation and the European Research Council under the Seventh Framework Program of the European Community (FP720072013; ERC Grant Agreement No. 307535). The NSF is gratefully acknowledged for support for the acquisition of an X-ray diffractometer (CHE-1725028).

REFERENCES

- Gandeepan, P.; Mueller, T.; Zell, D.; Cera, G.; Warratz, S.; Ackermann, L., 3d Transition Metals for C-H Activation. *Chem. Rev.* 2019, 119, 2192-2452.
- Shang, R.; Ilies, L.; Nakamura, E., Iron-Catalyzed C-H Bond Activation. Chem. Rev. 2017, 117, 9086-9139.
- 3. Ilies, L.; Nakamura, E., Iron-catalyzed C-H bond activation. *Top. Organomet. Chem.* **2016**, *56*, 1-18.
- White, M. C.; Zhao, J., Aliphatic C-H Oxidations for Late-Stage Functionalization. J. Am. Chem. Soc. 2018, 140, 13988-14009.
- Wang, P.; Deng, L., Recent Advances in Iron-Catalyzed C-H Bond Amination via Iron Imido Intermediate. *Chin. J. Chem.* 2018, 36, 1222-1240.
- Milan, M.; Salamone, M.; Costas, M.; Bietti, M., The Quest for Selectivity in Hydrogen Atom Transfer Based Aliphatic C-H Bond Oxygenation. Acc. Chem. Res. 2018, 51, 1984-1995.
- 7. Norinder, J.; Matsumoto, A.; Yoshikai, N.; Nakamura, E., Iron-Catalyzed Direct Arylation through Directed C-H Bond Activation. *J. Am. Chem. Soc.* **2008**, *130*, 5858-5859.
- Cera, G.; Haven, T.; Ackermann, L., Expedient Iron-Catalyzed C-H Allylation/Alkylation by Triazole Assistance with Ample Scope. *Angew. Chem., Int. Ed.* 2016, 55, 1484-1488.
- Ilies, L.; Matsubara, T.; Ichikawa, S.; Asako, S.; Nakamura, E., Iron-Catalyzed Directed Alkylation of Aromatic and Olefinic Carboxamides with Primary and Secondary Alkyl Tosylates, Mesylates, and Halides. J. Am. Chem. Soc. 2014, 136, 13126-13129.
- Fruchey, E. R.; Monks, B. M.; Cook, S. P., A Unified Strategy for Iron-Catalyzed ortho-Alkylation of Carboxamides. J. Am. Chem. Soc. 2014, 136, 13130-13133.
- Loup, J.; Parchomyk, T.; Luelf, S.; Demeshko, S.; Meyer, F.; Koszinowski, K.; Ackermann, L., Mössbauer and mass spectrometry support for iron(II) catalysts in enantioselective C-H activation. *Dalton Trans.* 2019, 48, 5135-5139.
- 12. Gu, Q.; Al Mamari, H. H.; Graczyk, K.; Diers, E.; Ackermann, L., Iron-catalyzed C(sp²)-H and C(sp³)-H arylation by triazole assistance. *Angew. Chem., Int. Ed.* **2014,** *53*, 3868-3871.
- Shen, Z.; Cera, G.; Haven, T.; Ackermann, L., Tri-Substituted Triazole-Enabled C-H Activation of Benzyl and Aryl Amines by Iron Catalysis. *Org. Lett.* 2017, 19, 3795-3798.
- 14. Mo, J.; Mueller, T.; Oliveira, J. C. A.; Ackermann, L., 1,4-Iron Migration for Expedient Allene Annulations through Iron-Catalyzed C-H/N-H/C-O/C-H Functionalizations. *Angew. Chem., Int. Ed.* 2018, 57, 7719-7723.
- 15. Cera, G.; Haven, T.; Ackermann, L., Iron-catalyzed C-H/N-H activation by triazole guidance: versatile alkyne annulation. *Chem. Commun.* **2017**, *53*, 6460-6463.
- 16. Mo, J.; Muller, T.; de, O. J. C. A.; Demeshko, S.; Meyer, F.; Ackermann, L., Iron-Catalyzed C-H Activation with Propargyl Acetates: Mechanistic Insights on Iron(II) by Experiment, Kinetics, Mössbauer Spectroscopy and Computation. *Angew. Chem. Int. Ed.* 2019, Early View, doi: 10.1002/anie.201904110.
- 17. Cera, G.; Haven, T.; Ackermann, L., Iron-Catalyzed C-H Alkynylation through Triazole Assistance: Expedient Access to Bioactive Heterocycles. *Chem. Eur. J.* **2017**, *23*, 3577-3582.

- 18. Matsubara, T.; Asako, S.; Ilies, L.; Nakamura, E., Synthesis of Anthranilic Acid Derivatives through Iron-Catalyzed Ortho Amination of Aromatic Carboxamides with N-Chloroamines. J. Am. Chem. Soc. 2014, 136, 646-649.
- 19. Monks, B. M.; Fruchey, E. R.; Cook, S. P., Iron-catalyzed C(sp2)-H alkylation of carboxamides with primary electrophiles. *Angew. Chem., Int. Ed.* **2014,** *53*, 11065-11069.
- Ilies, L.; Asako, S.; Nakamura, E., Iron-catalyzed stereospecific activation of olefinic C-H bonds with Grignard reagent for synthesis of substituted olefins. J. Am. Chem. Soc. 2011, 133, 7672-7675.
- 21. Shang, R.; Ilies, L.; Matsumoto, A.; Nakamura, E., β-Arylation of Carboxamides via Iron-Catalyzed C(sp3)-H Bond Activation. *J. Am. Chem. Soc.* **2013**, *135*, 6030-6032.
- Shang, R.; Ilies, L.; Nakamura, E., Iron-Catalyzed Directed C(sp2)-H and C(sp3)-H Functionalization with Trimethylaluminum. J. Am. Chem. Soc. 2015, 137, 7660-7663.
- 23. Aguilar, D.; Cuesta, L.; Nieto, S.; Serrano, E.; Urriolabeitia, E. P., Orthometallation as a strategy in Pd-mediated organic synthesis. *Curr. Org. Chem.* **2011**, *15*, 3441-3464.
- 24. Sun, Y.; Tang, H.; Chen, K.; Hu, L.; Yao, J.; Shaik, S.; Chen, H., Two-State Reactivity in Low-Valent Iron-Mediated C-H Activation and the Implications for Other First-Row Transition Metals. J. Am. Chem. Soc. 2016, 138, 3715-3730.
- Neidig, M. L.; Carpenter, S. H.; Curran, D. J.; DeMuth, J. C.; Fleischauer, V. E.; Iannuzzi, T. E.; Neate, P. G. N.; Sears, J. D.; Wolford, N. J., Development and Evolution of Mechanistic Understanding in Iron-Catalyzed Cross-Coupling. Acc. Chem. Res. 2019, 52, 140-150.
- Sears, J. D.; Neate, P. G. N.; Neidig, M. L., Intermediates and Mechanism in Iron-Catalyzed Cross-Coupling. *J. Am. Chem. Soc.* 2018, 140, 11872-11883.
- 27. Munoz, S. B.; Daifuku, S. L.; Brennessel, W. W.; Neidig, M. L., Isolation, Characterization, and Reactivity of Fe₈Me₁₂-: Kochi's S = 1/2 Species in Iron-Catalyzed Cross-Couplings with MeMgBr and Ferric Salts. *J. Am. Chem. Soc.* 2016, 138, 7492-7495.
- 28. Daifuku, S. L.; Kneebone, J. L.; Snyder, B. E. R.; Neidig, M. L., Iron(II) Active Species in Iron-Bisphosphine Catalyzed Kumada and Suzuki-Miyaura Cross-Couplings of Phenyl Nucleophiles and Secondary Alkyl Halides. *J. Am. Chem. Soc.* 2015, *137*, 11432-11444.
- 29. Kneebone, J. L.; Brennessel, W. W.; Neidig, M. L., Intermediates and Reactivity in Iron-Catalyzed Cross-Couplings of Alkynyl Grignards with Alkyl Halides. *J. Am. Chem. Soc.* **2017**, *139*, 6988-7003.
- 30. Albrecht, M., Cyclometalation Using d-Block Transition Metals: Fundamental Aspects and Recent Trends. *Chem. Rev.* **2010**, *110*, 576-623.
- 31. Gutlich, P.; Bill, E.; Trautwein, A. X., Mössbauer Spectroscopy and Transition Metal Chemistry: Fundamentals and Applications. Springer-Verlag: Berlin, 2011.
- 32. Pavel, E. G.; Kitajima, N.; Solomon, E. I., Magnetic Circular Dichroism Spectroscopic Studies of Mononuclear Non-Heme Ferrous Model Complexes: Correlation of Excited- and Ground-State Electronic Structure with Geometry. J. Am. Chem. Soc. 1998, 120, 3949-3962.
- Daifuku, S. L.; Kneebone, J. L.; Snyder, B. E. R.; Neidig, M. L., Iron(II) Active Species in Iron–Bisphosphine

- Catalyzed Kumada and Suzuki–Miyaura Cross-Couplings of Phenyl Nucleophiles and Secondary Alkyl Halides. *J. Am. Chem. Soc.* **2015**, *137*, 11432-11444.
- 34. Fleischauer, V. E.; Munoz, S. B., III; Neate, P. G. N.; Brennessel, W. W.; Neidig, M. L., NHC and nucleophile chelation effects on reactive iron(II) species in alkyl-alkyl cross-coupling. *Chem. Sci.* **2018**, *9*, 1878-1891.
- 35. Isobe, M.; Kondo, S.; Nagasawa, N.; Goto, T., Trialkylzinclithium [R3ZnLi]. A new reagent for conjugate
- addition to α,β -unsaturated ketones. *Chem. Lett.* **1977**, 6, 679-82.
- 36. Neese, F.; Solomon, E. I., MCD C-Term signs, saturation behavior, and determination of band polarizations in randomly oriented systems with spin $S \ge 1/2$. Applications to S = 1/2 and S = 5/2. *Inorg. Chem.* **1999**, *38*, 1847-1865.

TOC FIGURE

